Impact behavior of model porous concretes

Agar Ozbek, Ayda Safak; Weerheijm, Jaap; van Breugel, Klaas

DOI
10.1617/s11527-019-1388-z

Publication date
2019

Document Version
Accepted author manuscript

Published in
Materials and Structures/Materiaux et Constructions

Impact Behavior of Model Porous Concretes

Ayda Safak Agar Ozbek[a,*] Jaap Weerheijm[b,c], Klaas van Breugel[b]

[a] Faculty of Civil Engineering, Istanbul Technical University, Istanbul, Turkey
sagar@itu.edu.tr, +905557244316
[b] Faculty of Civil Engineering and Geosciences, Delft University of Technology, Delft, The Netherlands
[c] TNO, Defense, Security and Safety, Rijswijk, The Netherlands

Keywords: Porous concrete, impact, finite element analysis, explicit

Abstract

In this work, findings of a numerical study performed to investigate the impact behavior of porous concrete, modeled as a four phase cementitious composite consisting of aggregates, cement paste, interfacial transition zones (ITZ) and air, are presented. The numerical analyses contributed to the process of designing a special type of concrete for safety purposes i.e. as a protective building material to be used in safety walls outside important buildings or munition magazines for storing explosives. In case of an explosion, large concrete fragments that are formed, cause a very important threat. Therefore, in the scope of a research project, designing a special type of concrete having sufficient strength, but fracturing into small fragments under impact loading was aimed. In the numerical analyses, model porous concretes, in which the amounts and properties of pores and aggregates could be varied individually, were used to see the sole effect of each parameter. According to the results, it was found that at constant total porosity, the impact strength increased with decreasing pore size while multiple fragmentation was observed. On the other hand, the impact strengths of porous concretes with different size aggregates (with constant total aggregate content and porosity) were approximately the same

when no interfacial transition zone (ITZ) was defined. However, when ITZ was present, the impact strength was found to decrease as the aggregates were finer. This trend was also valid for the respective full concretes. Representative experimental results of porous concretes were also presented in order to support the numerical results.

1. Introduction

Modeling tools provide important insight into how a material behaves, complementary to experimental approaches. Various modeling and simulation techniques are being used by researchers in order to better understand the factors that control the properties of cementitious materials [1, 2]. As a part of a research project on designing porous concretes that fracture into small size fragments under impact loading, to be used in safety structures such as protective walls outside important buildings and storages for explosives, the dynamic behavior of porous concrete was numerically analyzed [3, 4]. In an explosion, in addition to the explosive itself, large concrete fragments fractured from a concrete structure cause a very important threat. Therefore, in the scope of a research project, designing a cementitious building material fracturing into small fragments under impact loading, while having sufficient strength, was aimed. Porous concrete is a construction material, that is used efficiently in various applications, owing to its favorable properties as a pavement, drainage and water purification material. Therefore, it is being investigated thoroughly by researches in terms of its content, production method and pore structure [5-8]. Its dynamic properties on the other hand have not been investigated widely due to its weakened mechanical properties as a consequence of its intentionally increased meso-scale porosity. In the research project, the impact properties of porous concrete have been investigated with an intent to reduce the fragment sizes while also enhancing the impact strength. Therefore, the parameters that affect the impact strength and

fragmentation behavior of porous concrete were analyzed. In the design process, numerical findings, in terms of the effects of different material phases on the impact behavior of porous concrete, determined the research direction.

Several researchers have investigated the stress concentrations around a hole in brittle porous solids and have been able to quantify the high stress concentrations at the vicinity of the pores both analytically and numerically [9-13]. Stress concentrations and their locations are very important because these amplified stresses are usually the causes of cracks emanating from those locations. Additionally, because in real materials, pores are usually not bounded by smooth surfaces, the stress concentrations are expected to be even much higher [10]. In a related study focusing on the behavior of materials containing pores, a series of uniaxial compression tests on samples containing a single hole with different diameters and sample widths were conducted. In the study, it was found that high tensile stresses were formed at the poles and that the magnitude of the stresses around the hole was greatly influenced by the location and the diameter of the hole and the sample width [11]. In a numerical study, the influence of hole diameter on the crack growth behavior was examined and it was found that the crack initiation and growth in the specimen with the smallest hole is much more difficult at the early stage of loading. For the specimens containing larger holes the cracks initiate earlier and have a higher growth rate at the beginning [14]. In another study, it was seen that the distance between the hole and the specimen boundary was also very effective on the stress state formed [15]. In the pioneering work of Ashby and Sammis, the influence of the state of confinement on the failure mechanisms of porous materials was investigated. It was stated that in brittle porous solids, unconfined samples tend to fail by vertical slabbing, where microcracks propagate and percolate to form failure planes parallel to the loading direction [16]. In another study, where again the fracture of porous

materials was investigated, a fracture criterion involving both toughness and strength was proposed. In the study, the controversy between the crack blunting due to the presence of pores, resulting in an apparent toughness enhancement and the weakening effect caused by the increasing volume fraction of pores was emphasized [17].

In porous concrete, pores that are intentionally incorporated in the material drastically affect the mechanical behavior as expected. The pore structure of porous concrete on the other hand is controlled by several different parameters e.g. aggregate grading, amount of cement paste, compaction etc. Because in a real material the effects of various parameters are coupled, extracting the sole effect of a single parameter cannot sometimes be possible in case of analyzing real porous concretes. Therefore, virtual or model concretes were analyzed in this work, where the size, amount and distribution of the pores as well as the aggregate sizes could individually be varied. In the analyses that also included aggregates, the effect of the interfacial transition zones (ITZ) between the cement paste and aggregate phases was also investigated.

In the scope of the research project, design and production of various porous concretes having static strengths at the range of 30-50 MPa and drop weight impact strengths about 65-85 MPa were accomplished by adjusting the mixture design and applying enhanced compaction [4]. In order to see the effects of aggregate grading, porosity and pore size distribution on the results, in the mixtures presented in this current work, the aggregates were selected to be either in one (2-4 mm or 4-8 mm) or two (2-4 mm and 4-8 mm, each 50 percent by mass) standard size ranges i.e. three different aggregate gradings. The rest of the composition was mostly kept constant. The details of the compositional properties of the selected representative porous concrete mixtures as well as the experimental results presented in order to support the numerical results are provided in Online Resource 1. On the other hand, the high speed photography and computed tomography

images of the porous concretes under dynamic and static loading provided important information on the fracturing behavior of porous concretes, which were also included in Online Resource 1. According to the experimental results, it was found that decreasing the aggregate size or using two sizes of aggregates instead of single size had an increasing effect on the impact strengths. While the aggregate grading and pore size distribution are coupled parameters, decreasing the total porosity or the pore size (at constant total porosity) also increased the impact strength of porous concretes. Aggregate and pore sizes and their distributions had a major influence on the fragmentation performances of porous concretes as well. The details of the experimental findings, which support the numerical analyses, are explained in more detail in Online Resource 1.

2. Finite Element Analyses of the Dynamic Behavior of Porous Concrete

In this work, finite element analyses were conducted to investigate the dynamic responses of different types of model porous concretes at a drop weight impact test [3,4]. Drop weight impact test was selected because drop weight tests were actually conducted in the scope of the experimental part of the related research project. They were fast and direct tests to investigate the impact properties of the porous concretes designed. In the analyses, finite element analysis software ABAQUS/Explicit (explicit dynamic analysis module) was used. In choosing an approach to a nonlinear dynamic problem, the length of time of the response, the sources of nonlinearity as well as the size of the problem are usually considered. In this study, the explicit time integration analysis was chosen over the implicit analysis especially due to the short duration of impact, the large deformations and the nonlinear material response. The explicit integration method also carries the advantage of efficiently solving highly discontinuous events and is therefore, often selected because of its efficiency in solving complicated contact problems

[18]. In the explicit finite element analysis, because the explicit scheme is incremental, but not iterative, the results are not automatically checked for accuracy. The time step to be used is therefore very critical in terms of the stability of the solution. Thus, in most cases, accuracy is not of concern, because the stability condition already imposes a very small time increment such that the solution changes only slightly in a time increment. While the analysis may take a very large number of increments, each increment is relatively inexpensive, resulting in an economical solution [19-21]. In the explicit analyses conducted on porous concretes in this research, the time steps were typically at the scale of 10^{-14}-10^{-15} sec.

Initially, to be able to more clearly see the effect of a pore on the behavior of the material, dynamic analyses were conducted on plain concrete (modeled as a one phase material with average concrete properties) containing a single hole. Subsequently, porous concretes containing regularly distributed multiple holes and randomly distributed multiple holes were analyzed. To investigate the effect of aggregates, model porous and normal concretes with circular aggregates having different diameters, with and without ITZ phases were also analyzed. The main features of the analyses conducted on model concretes are given in Tables 1 and 2 in the respective sections.

In the analyses, the aggregate phase was identified as linear elastic. The Concrete Damaged Plasticity (CDP) model, which is a plasticity-based damage model, was used to define the different cementitious phases analyzed, i.e. plain concrete, interfacial transition zone (ITZ) and bulk cement paste. The CDP model is based on isotropic damaged elasticity in combination with isotropic tensile and compressive plasticity to define the inelastic behavior of concrete [21-25]. It includes two main mechanisms which are the tensile cracking and the compressive crushing of the concrete material, i.e. different degradations of the elastic stiffness in tension and

compression are considered. Rate sensitivity is also present in the model which enables dynamic analysis. The model is well established and documented in literature [21, 26-29].

Change in volume due to plasticity is defined by a plastic potential function, G in the model [21, 22]. The evolution of the inelastic displacements in the fracture process zone is defined through the flow rule. Similar to other plasticity models, there are three criteria associated with the model. A yield surface at which plastic deformation begins, a hardening rule and a flow rule, which defines the plastic stress-strain relation. The plasticity yield surface implemented in ABAQUS is devised by Lubliner, et al (1989) and modified by Lee and Fenves (1998) [22, 23]. The yield criterion is calibrated with uniaxial tension and compression. A non-associated flow rule is assumed in the CDP model, where the yield function and the plastic potential do not coincide. This is important for realistic modeling of the volumetric expansion under compression for frictional materials such as concrete [30]. The flow potential adopted in the model is the Drucker–Prager hyperbolic function based on the dilation angle, the uniaxial tensile stress at failure and eccentricity. The plastic dilation angle is directly related to the slope of plastic volumetric strain [31]. In addition, the volume of voids increases dramatically causing a rapid dilation of the volume of the whole concrete.

When the material flows inelastically, the in elastic part of the deformation is defined by the flow rule [21]:

$$\dot{\varepsilon}^{pl} = \dot{\lambda}\frac{\partial G(\bar{\sigma})}{\partial \bar{\sigma}}$$

where G is the flow potential, $\dot{\lambda}$ is the nonnegative plastic multiplier. The plastic-damage model assumes nonassociated potential flow.

$$G = \sqrt{(\epsilon\sigma_{t0}tan\psi)^2 + \bar{q}^2} - \bar{p}tan\psi$$

where ψ is the dilation angle measured in the p-q plane at high confining pressure; σ_{t0} is the uniaxial tensile stress at failure and ϵ is a parameter based on eccentricity, that defines the rate at which the function approaches the asymptote. The flow potential approaches a straight line as the eccentricity tends to zero. The function asymptotically approaches the linear Drucker-Prager flow potential at high confining pressure stress [21].

In the model, experimental stress-stain data of the cementitious phases, i.e. the ITZ and cement paste, can be used as input. However, when used directly as input to define the properties of the cementitious phases, raw experimental stress-stain data causes error in the program because small fluctuations in the experimental graphs can sometimes give negative plastic strain values during computation. Therefore, all the user-provided experimental stress versus inelastic strain curves are smoothened and checked according to the format accepted by the program, by also taking the widely accepted works of Jankowiak and Lodygowski and Lubliner et al. as reference [21, 22, 26].

An axisymmetric geometry was defined in the analyses. The dimensions of the mesh representing the concrete sample was 30 mm in width, 75 mm in height (corresponding to 60 mm diameter and 75 mm height sample when rotated axisymmetrically). The mesh of the steel impactor had 55 mm width and 220 mm height (corresponding to the 110 mm diameter and 220 mm height impactor when rotated). The drop weight impact test setup, which was defined in the simulations, consisted of a stationary steel base structure at the bottom, the concrete sample and the steel impactor. A typical finite element mesh for a porous concrete impact computation is shown in Fig. 1. Steel material was defined as linear elastic with elastic constants of: E=200 GPa and ν=0.3. The elements used in the analyses were 0.2 mm x 0.2 mm reduced integration, axisymmetric elements (CAX4R in ABAQUS).

A fixed boundary was defined at the bottom surface of the steel base structure. The displacement in x-direction and the rotation were constrained for the impactor. The steel-concrete contacts formed between the steel base structure and the bottom surface of the concrete sample and between the steel impactor and the top surface of the sample were defined as surface-to-surface contacts with a friction coefficient of 0.3 in tangential direction. The concrete-concrete contacts formed between the pore and fracture surfaces of the porous concrete sample were defined as "self-contact" with a friction coefficient of 0.5 [32-34]. Self-contact is used when the outer surfaces of a deformable layer come into contact. The axial impact loading applied to the concrete sample was defined as an initial velocity (4.5 m/sec) that has been assigned to the impactor, which was approximately the velocity that was measured using laser Doppler velocimetry during the experiments [4]. The parameters that were focused on in the analyses were mainly the impact strengths and crack patterns estimated by the damage contours. These parameters enabled the evaluation of different porous concrete options in terms of strength and fragmentation behavior.

3. Numerical Analysis Results

3.1. Model Porous concrete with a Single Pore

In order to more clearly see the stress and damage distributions around a hole, numerical analyses were initially conducted on a 60 mm diameter-75 mm height concrete cylinder, that contains a single pore, under impact loading. The pore diameter was 16.27 mm. In this analysis, the matrix material was taken as a single phase material (similar to the solid phase of porous concrete, which does not contain any fine aggregates, but only coarse aggregates) where concrete properties were defined using the CDP model. In the model, the following parameters were defined: E=35 GPa, ν=0.19. The modulus of elasticity of porous concrete is high due to the high

percentage of aggregates in the material and the low ITZ content due to the lack of fine aggregates. The rest of the parameters needed for the model, that cannot commonly be measured in experiments (such as dilation angle and viscosity parameter), were taken from the widely referenced work of Jankoviak and Lodygowski [26]. The same input data for plain concrete was also used for representing the material properties of the plain concrete material in the model porous concretes containing (regularly and randomly distributed) circular pores in sections 2.2 and 2.3.

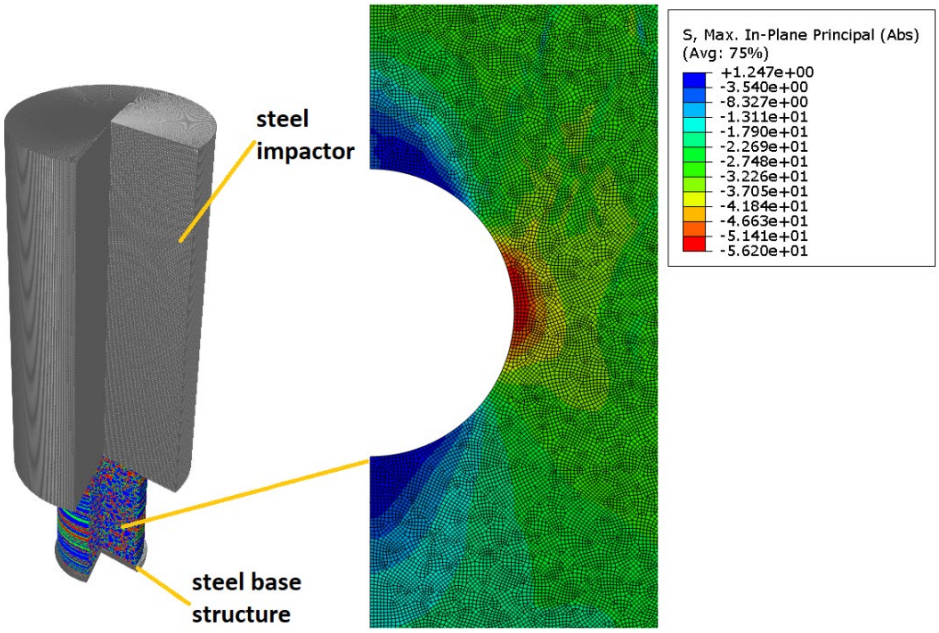

Fig. 1 Stress concentrations around a hole in a concrete cylinder (under impact)

In Fig 1, the stress distributions around a single hole in the cylindrical plain concrete specimen are shown. To check the stress concentrations altogether, the absolute maximum principle stress was selected to see the largest value of the minimum and maximum principals regardless of their signs. In the figure, high tensile stresses at the poles and compressive stresses at the two sides of the pore can clearly be observed. Very similar contours were also observed for the damage distribution analyses.

3.2. Model Porous Concretes with Regularly Distributed Circular Pores

Model porous concretes having circular pores of different radii, pore size distributions and total porosities were analyzed to see the effect of those parameters individually. The main features of the analyses conducted are given in Table 1. In the analyses, concretes with four different numbers of pores (8, 23, 77 and 281) were investigated. Concrete Damaged Plasticity (CDP) model was again used to define the concrete phase. The input data used for the solid phase of model porous concretes were the same as in the single pore analyses.

In the first set of analyses, samples with regularly distributed circular pores were investigated. Initially, the effect of pore size was analyzed while the total porosities were kept constant. A representative set of meshes (total porosity 0.1005) is presented in Fig.2. The impact responses of model porous concretes with pores of different sizes, but constant total porosities of 0.1005, 0.1786 and 0.2791 were compared. According to the analysis results, it could be concluded that the impact strength increased as the pore size decreased while the total porosity was kept constant. This trend was found to be valid for all the total porosities analyzed, i.e. 0.1005, 0.1786 and 0.2791.

Table 1. Analyses conducted on model porous concretes with circular pores

MODEL POROUS CONCRETES WITH CIRCULAR PORES (Each analysis repeated also for the no end friction option) Material Phases: Plain Concrete + Air				
Analysis Label	N. of Pores	Pore Radius (mm)	Porosity	Pore Distribution
REGPORE8NO1	8	3.0	0.1005	Regular
REGPORE8NO2		4.0	0.1786	Regular

REGPORE8NO3		5.0	0.2791	Regular
REGPORE23NO1	23	1.7693	0.1005	Regular
REGPORE23NO2		2.3591	0.1786	Regular
REGPORE23NO3		2.9488	0.2791	Regular
REGPORE77NO1	77	0.9670	0.1005	Regular
REGPORE77NO2		1.2893	0.1786	Regular
REGPORE77NO3		1.6116	0.2791	Regular
REGPORE281NO1	281	0.5062	0.1005	Regular
REGPORE281NO2		0.6749	0.1786	Regular
REGPORE281NO3		0.8436	0.2791	Regular
RANDPORE8NO1	8	3.0	0.1005	Random1
RANDPORE8NO2				Random2
RANDPORE8NO3				Random3
RANDPORE8NO4				Random4
RANDPORE23NO1	23	1.7693	0.1005	Random1
RANDPORE23NO2				Random2
RANDPORE23NO3				Random3
RANDPORE23NO4				Random4
RANDPORE77NO1	77	0.9670	0.1005	Random1
RANDPORE77NO2				Random2
RANDPORE77NO3				Random3
RANDPORE77NO4				Random4
RANDPORE281NO1	281	0.5062	0.1005	Random1
RANDPORE281NO2				Random2
RANDPORE281NO3				Random3
RANDPORE281NO4				Random4

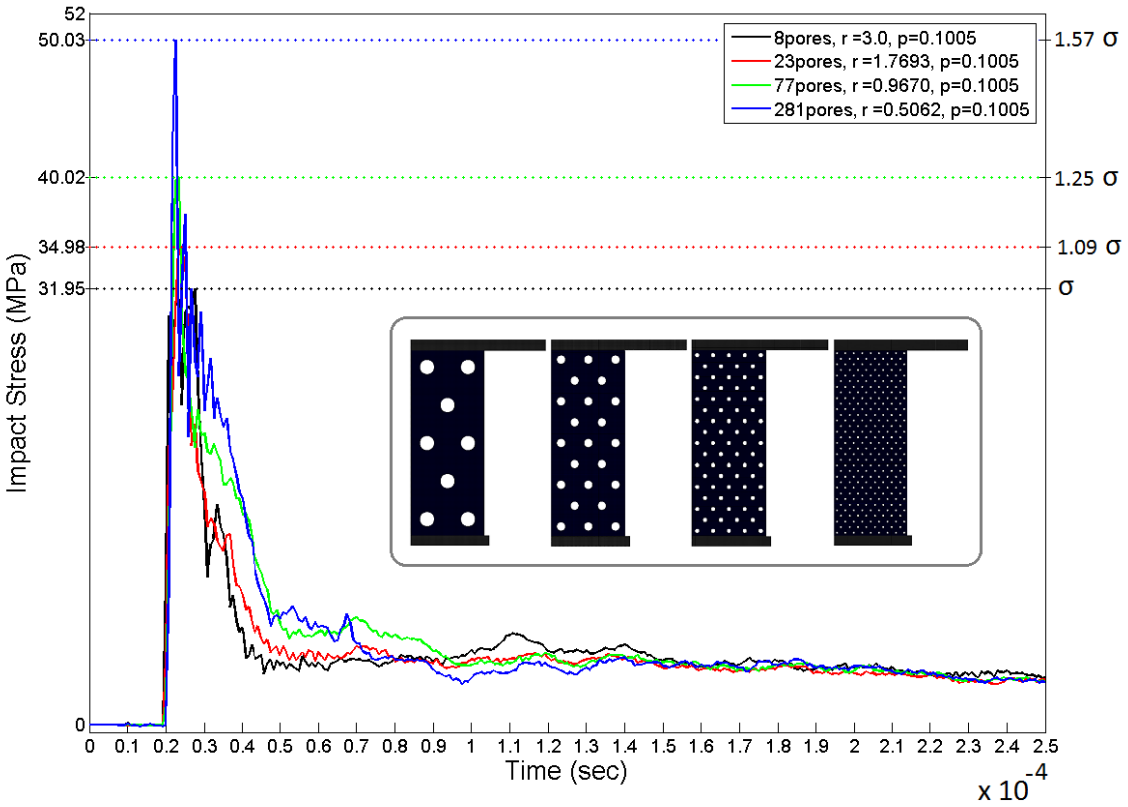

Fig. 2 Impact stress time histories of model porous concretes with different pore sizes (total porosity 0.1005)

This outcome provided an important research direction to be followed in the design process of enhanced strength, multiple fragmenting porous concretes. Additional data on how this outcome was valid also for other total porosities, which were again kept constant while the pore size was varied, are presented in Online Resource 2.

Along with the dynamic strengths, the fragmentation behaviors of the different mixtures were also important for this research. In the analyses, the crack growth under impact loading is visualized using the compressive and tensile damage variable contours (DamageC and DamageT) represented by a scalar value with a range of 0-1. The cracks generated in the specimen are presented for selected time steps showing the compressive and tensile damage separately. The occurrence of damage due to compression is usually observed later in time

compared to damage due to tension as expected. As it will also be observed in the damage contours of the following model concretes, the cracks originating from the pores due to tension or compression are then guided by not only material based, but also structural effects such as restrained lateral deformations due to boundary conditions. Due to the friction between the steel base structure at the bottom and the bottom surface of the concrete specimen as well as the friction between the top surface of the specimen and the bottom surface of the impactor, the initial cracks become inclined and curved wing cracks develop from the crack-tips. This mechanism is also observed in numerous studies performed on homogeneous brittle materials such as PMMA [35]. While all model concretes were examined in terms of damage, the damage results of 281 pore concrete were demonstrated in Fig. 3 to represent the damage behaviors of porous concretes. The elements with a damage value of 0.9 or higher were removed from the contour for the estimation of the crack patterns. The element removal applied is in the display to better visualize the cracking behavior, where the elements were actually not removed from the analysis. The images showing the results at a selected instance: $5.0*10^{-5}$ sec, which is close to the end of the descending branch (see Fig.2), were presented. Because the finite element mesh is very fine, the colored contours are not visible in the images that show the whole mesh. Therefore, a piece of zoomed image showing a close up view was also added to the figure. At the zoomed image, elements with damage values of 0.9 or higher were not removed. The last contour plot in each figure gives the combination of tensile and compressive damage contours (for $5.0*10^{-5}$ sec), which reflects a more realistic crack pattern.

The dynamic fracturing behaviors observed in these analyses involve both material and structural aspects. The cracks that originate from the top and bottom poles of the pores in the tensile damage graphs are clearly seen in Fig. 3. They are the typical tensile damage locations that can

be expected at the vicinity of pores. Additional tensile splitting cracks emanating from those locations are also visible. In the compressive damage contours, the cracks, that originate from the sides, propagate further by making inclinations. State of triaxial compression exists due to boundary effects in impact testing. Friction between the concrete sample and the steel impactor or the steel base structure of the setup causes lateral compression additional to the uniaxial compression component. Therefore, limited and sometimes no damage can be seen in the triaxially loaded zones at the border of the samples.

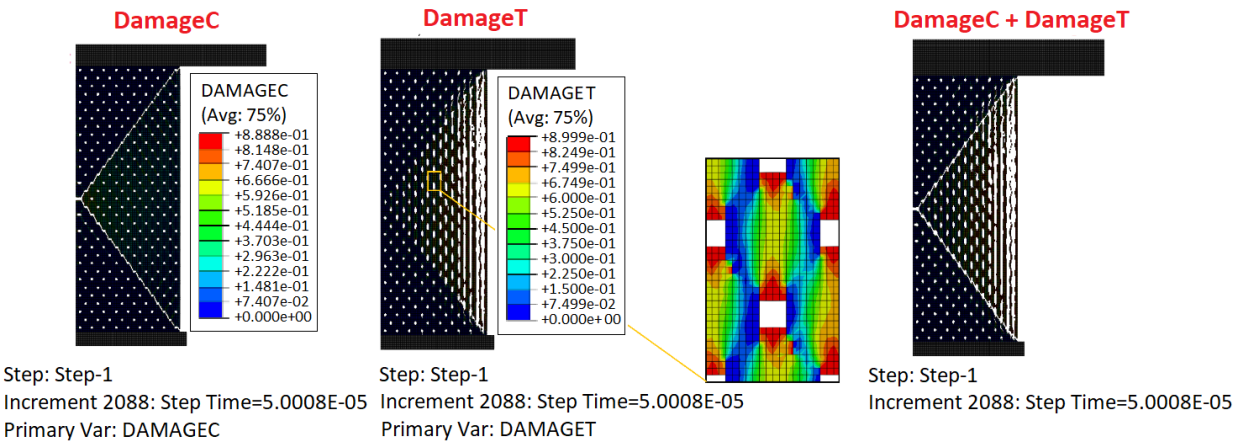

Fig. 3 Compressive (upper images) and tensile (bottom images) damage contours and their combination for estimating the crack distribution under impact loading (281 pores, r=0.5062 mm, porosity=0.1005) (elements with DamageC or DamageT > 0.9 removed)

When the fragmentation behaviors of the two model porous concretes with 8 and 281 pores were compared, an important difference could be observed. A multiple crack pattern has developed in the model concrete with 281 pores (see Fig. 3). This facilitated the formation of smaller-sized fragments, except in the triaxially confined zones. On the contrary, in the concrete with 8 pores, (provided in Online Resource 3) due to the presence of cracks at a very limited number of specific locations, comparatively large fragments could be estimated from the damage results. It should additionally be noted that even though the total porosity in both analyses was constant (0.1005), the impact strength of 281 pore concrete was 50.03 MPa, while that of the 8 pore

concrete was 31.95 MPa. Therefore, as an important trend that was used for designing an enhanced strength porous concrete fracturing into small fragments, it was found that as the pore size decreases, the sizes of the fragments drastically decrease while the dynamic strength increases. This trend was valid for all the analyses conducted for this set of model porous concretes.

In the next set of analyses, it was seen that increasing the pore size and consequently increasing the porosity, highly decreases the dynamic strength, as expected. This outcome was seen in all the four groups of samples (with 8, 23, 77 and 281 pores) analyzed. Decreasing the porosity from 0.2791 to 0.1005 in model concretes having 8 pores (decreasing the pore radius from 5 to 3 mm) enhances the impact strength 2.47 times. In case of samples with 281 pores the same decrease in porosity (by decreasing the pore radius from 0.8436 to 0.5062 mm) increases the dynamic strength 2.22 times. Similarly, for the pore sizes of 23 and 77, the ratios of increase in dynamic strengths were 2.46 and 2.19, respectively. Therefore, it is concluded that changing the porosity drastically affects the strength. For the porosities analyzed, this effect is nearly independent of the pore size.

3.3. Model Porous Concretes with Randomly Distributed Circular Pores

After investigating the individual effects of pore size and porosity on the performance of model concretes, random distribution should also be introduced in the model as an influencing parameter because in real porous concretes, the pores are far from being regularly distributed. The main features of the analyses conducted on model porous concretes with randomly distributed circular pores are also given in Table 1. In the analyses of model porous concretes with randomly distributed pores, again four mixtures with different numbers of pores options, namely 8, 23, 77 and 281 pores, were investigated. This time one pore size was selected to be

analyzed for each number of pores (r=3 mm, 1.7693 mm, 0.97670 mm and 0.5062 mm, respectively). Total porosity was kept constant at 0.1005. For each number of pores, four different random pore distributions were generated using the random number generator in MATLAB to determine the coordinates of the centers of the pores.

It was clearly seen in the experiments on porous concrete [4] and in the model concretes with regularly distributed pores that the boundary conditions have a strong effect on the fragmentation behavior. Therefore, in these analyses two different friction conditions were defined at the specimen boundaries. Friction coefficients of 0.3 (the same as in the analyses of model concretes with regularly distributed pores) and 0 (ideal testing with no friction) were used. The no friction analyses were conducted to better monitor the fragmentation behavior of the material itself, where the structural effects due to the constraining near the specimen boundaries were mitigated. It should however be indicated here that in the scope of this research, size effect has not been investigated. Size effect can expected to be highly valid for porous concrete.

The impact stress-time histories of the four random and one regularly distributed 8, 23, 77 and 281 pore concretes were examined along with the standard deviations of the peak values. Two representative sets of graphs are shown in Figs 4 and 5. It was seen that when the pore size increases, i.e. when the number of pores decreases, the effect of randomness on the results (the variance of impact strength) increases. At constant total porosity, when the sizes of the pores decrease (as the number of pores increases, e.g. for 281 pores as seen in Fig. 5) the material becomes more isotropic (compared to e.g. 8 pore option in Fig. 4). Even when there is a random pore distribution, this trend does not change. Consequently, the impact strength shows less scatter. The standard deviation of impact strength was found to be 2.26 MPa for samples with 281 pores, compared to 5.44 MPa for samples with 8 pores. When the friction at the top and

bottom boundaries were eliminated by defining a friction coefficient of 0, it was surprising to see that the impact strength results were not significantly affected and stayed approximately the same.

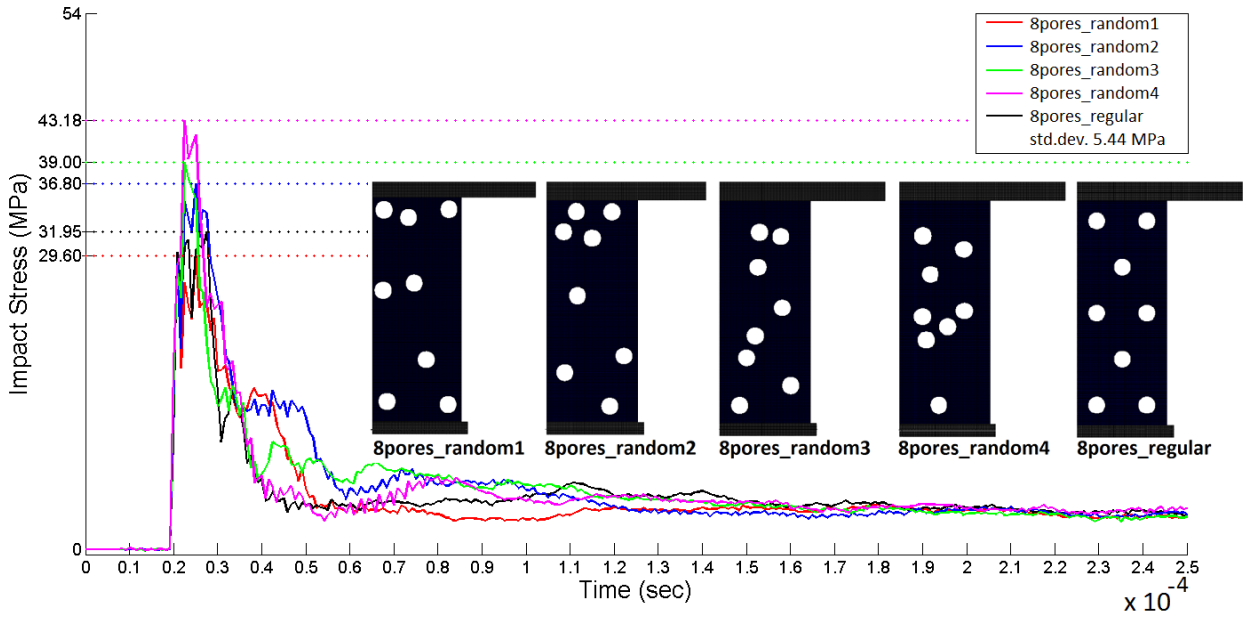

Fig. 4 Impact stress time histories of model concretes with 8 pores with four random distributions analyzed (with boundary friction)

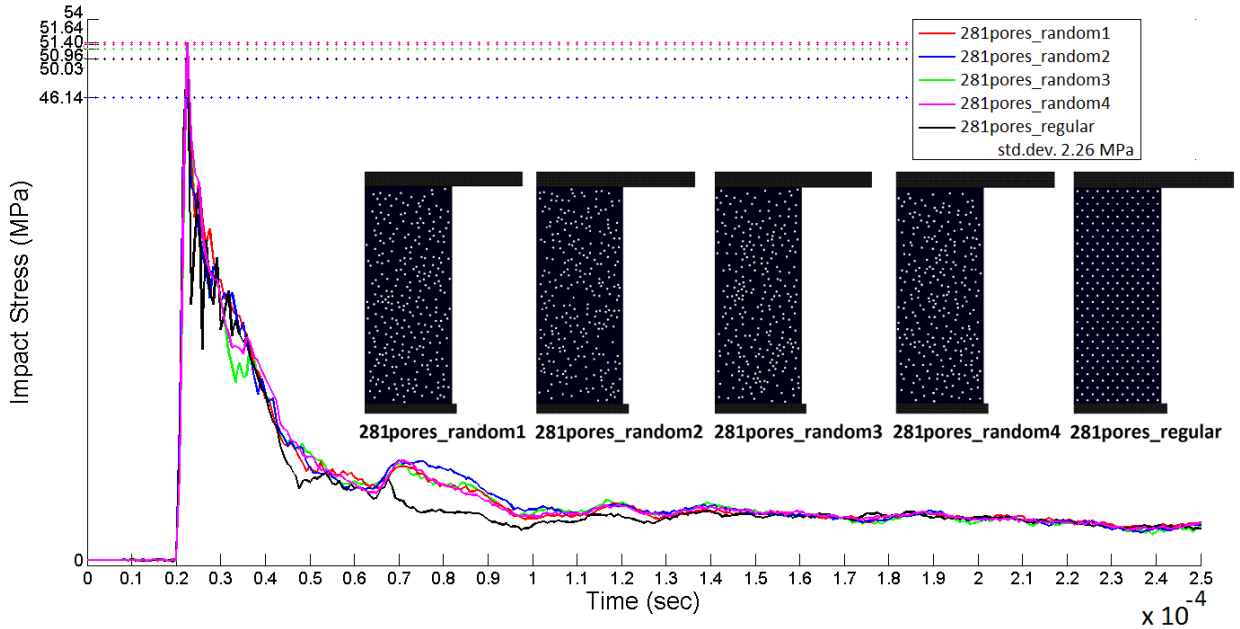

Fig. 5 Impact stress time histories of model concretes with 281 pores with four random distributions analyzed (with boundary friction)

The damage contours of two samples, with eight regularly or randomly distributed pores, are presented in Fig 6. The analysis results for damage distributions of all the concretes with 8, 23, 77 and 281 pores, both regularly and randomly distributed, are provided in Online Resource 4. In the representative image in Fig. 6, for samples with 8 pores, it is observed that when there is no friction, more tensile cracks oriented parallel to the compressive loading direction are formed. This kind of cracking is significantly different from the former inclined cracks caused by the state of triaxial compression at the specimen boundaries. In no friction analyses, while there are no triaxial confinement, the extensive tensile splitting causes the formation of small concrete columns that buckle and behave similar to columns fixed at both ends [36]. The splitting subsequently causes excessive dilation and ultimate failure. If the damage contour plots for different pore sizes in Online Resource 4 are compared, it is observed that for smaller pore size (i.e. as the number of pores increases), the fracture takes place in a similar way in concretes having different random pore distributions. Consequently, the shapes and the sizes of the fragments that are formed are similar. This is not the case for samples with large pores, where samples with different random pore distributions show very different fracture patterns, depending on the location of the pores (see the 8 pore model concrete in Fig. 6).

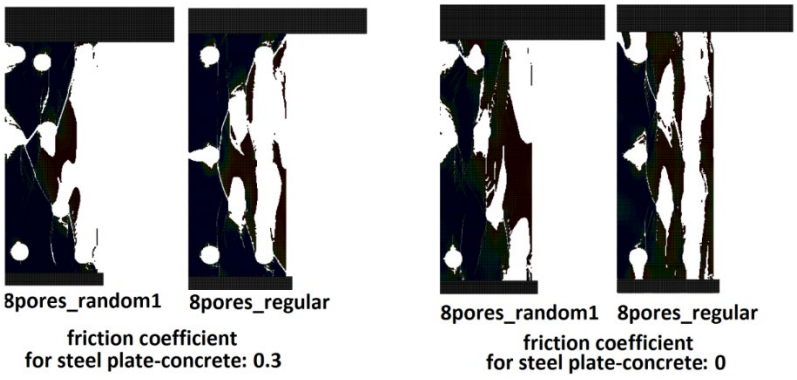

Fig. 6 Damage contours of model concretes with 8 pores with regular and one random distribution analyzed with and without boundary friction (elements with DamageC or DamageT > 0.9 removed)

3.4. Model Porous Concretes with Randomly Distributed Circular Pores and Aggregates

In order to see the effect of aggregates on the behavior of porous concretes, circular aggregates were also included in the analyses. The main features of the analyses conducted on model porous concretes with randomly distributed circular pores and aggregates are given in Table 2. Finite element meshes of model concretes containing aggregates are presented in Fig. 7.

Table 2 Analyses conducted on model concretes with circular pores and aggregates

MODEL POROUS/FULL CONCRETES WITH RANDOMLY DISTRIBUTED CIRCULAR PORES AND AGGREGATES Material Phases: Aggregates+(ITZ)+Bulk Cement Paste + Air						
Analysis Label	Presence of ITZ	N. of Aggregates	Aggregate Radius (mm)	N. of Pores	Pore Radius (mm)	Porosity
65AGG23PORE	no ITZ	65	1.7693	23	1.7693	0.10
5AGG23POREITZ	with ITZ					
65AGG (full concrete)	no ITZ	65	1.7693	0	0	0
65AGGITZ (full concrete)	with ITZ					
65AGG77POREITZ	with ITZ	65	1.7693	77	0.9670	0.10
218AGG23PORE	no ITZ	218	0.9670	23	1.7693	0.10
218AGG23POREITZ	with ITZ					
218AGG (full concrete)	no ITZ	218	0.9670	0	0	0
218AGGITZ (full concrete)	with ITZ					
218AGG77POREITZ	with ITZ	218	0.9670	77	0.9670	0.10

In these analyses, the effect of aggregate size on the dynamic behavior of porous concretes was investigated both when there is the ITZ phase present around the aggregates or not. In addition,

full concretes (without any pores) were also analyzed to further check the effect of aggregate size (with and without ITZ) on the impact behavior when pores are not present (see Fig. 4).

In all the concretes analyzed, the total amount of aggregate phase was kept constant (65 aggregates with r=1.7693 mm or 218 aggregates with r=0.9670 mm). The porosity was either 0.10 (the same as some of the porous concretes with circular pores presented in sections 2.2 and 2.3) or 0 (full concrete). The ITZ phase was defined in some of the selected concretes.

In the analyses, the aggregates were defined as elastic (with E=50 GPa, ν=0.3, taking basalt aggregates as reference). The bulk cement paste and ITZ phases around the aggregates were defined using the Concrete Damaged Plasticity model. The input data for the cement paste and ITZ phases were taken from the meso-scale ITZ and cement paste tests conducted in the scope of the research project [4]. The raw experimental strain data was slightly corrected to eliminate the local fluctuations and therefore to prevent program error, by taking the work of Jankoviak and Lodygowski as reference [21, 26]. The damage-inelastic strain input data were also taken from the same source. In the model, the following parameters were defined: E=30 GPa, ν=0.20 (for bulk cement paste), E=12.5 GPa, ν=0.15 (for ITZ).

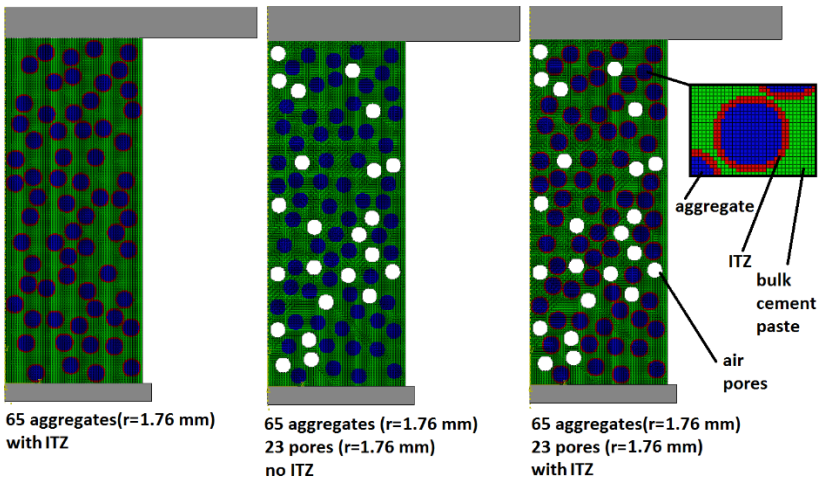

Fig. 7 Finite element meshes of model concretes with aggregates, with/without pores, and with/without ITZ

The representative meshes used in the analyses were presented in Fig. 7. The finite element meshes containing aggregates are presented in Online Resource 5 for better visualization of the samples, that have been numerically analyzed. The impact stress-time histories of porous concretes with 65 and 218 aggregate particles with ITZ are presented in Fig.8. With also the presence of ITZ, the impact strength of the porous concretes decreased as the number of aggregates were increased i.e. the sizes of the aggregates were decreased (while keeping the total amount of aggregates, the total porosity and the pore size constant). This outcome is valid for both 23 pore and 77 pore samples with 65 and 218 aggregates. For 23 pore samples, the difference between 65 and 218 aggregate concretes was even slightly more pronounced. For the same number of aggregates and same porosity, the impact strength increased as the pore size was decreased (from 23 pores with r=1.7693 mm to 77 pores with r=0.9670 mm) which was already emphasized in the analyses on model porous concretes with only circular pores in the previous sections.

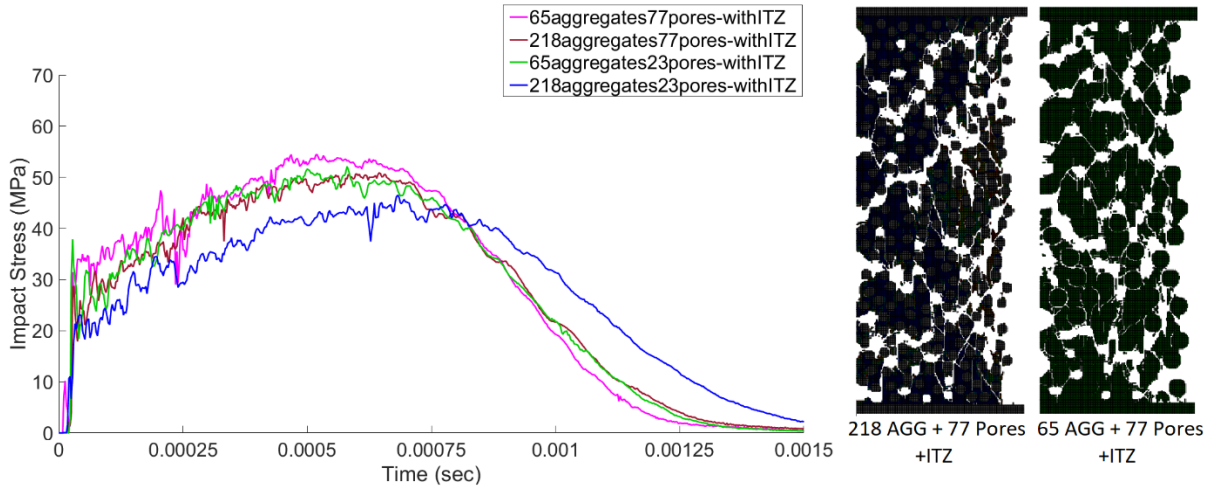

Fig. 8. Impact stress time history of model porous concretes with 65 and 218 circular aggregates and 23 and 77 circular pores, with ITZ and representative damage contours of two selected mixtures

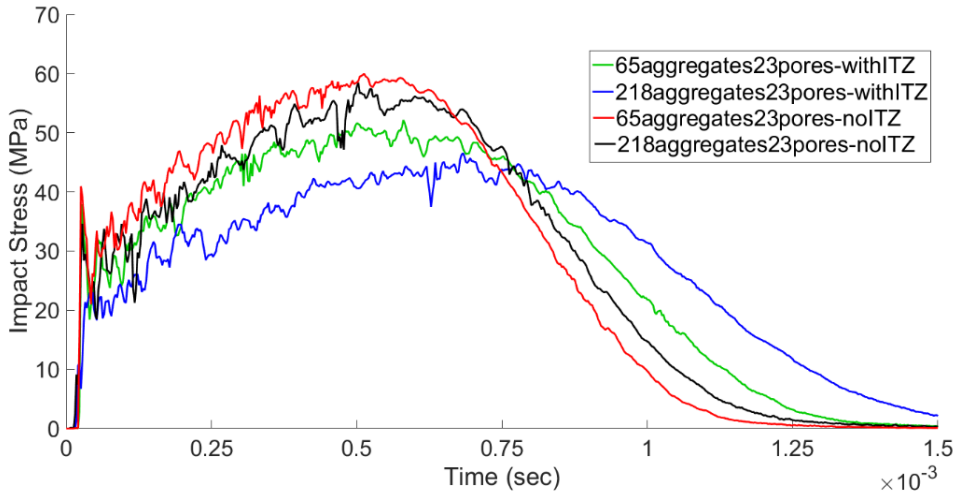

Fig. 9. Impact stress time histories of model porous concretes with 65 and 218 circular aggregates and 23 circular pores, with and without ITZ

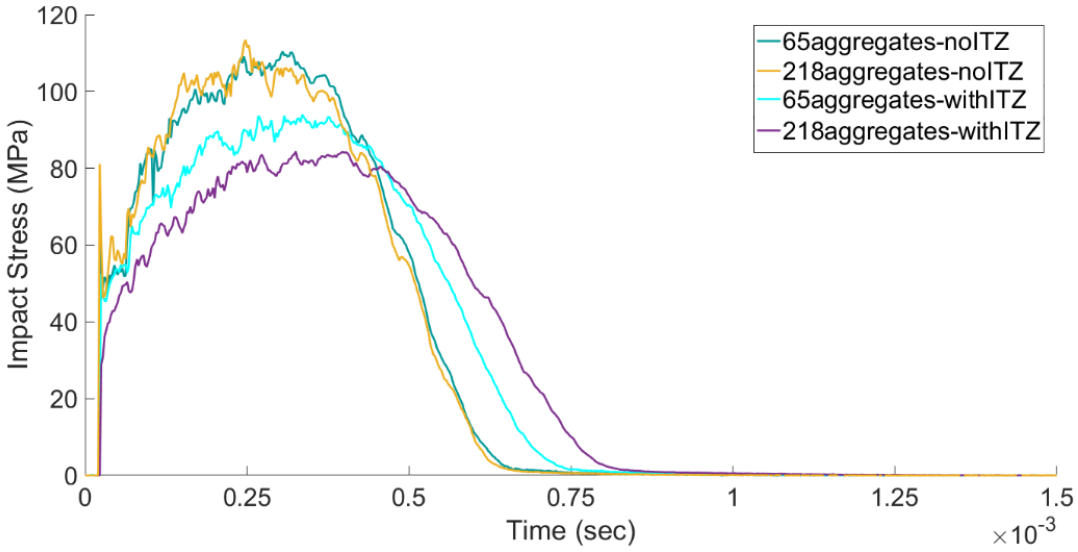

Fig. 10. Impact stress time histories of model full concretes with 65 and 218 circular aggregates, with and without ITZ

Due to the fact that as the aggregates get finer, the total amount of ITZ, which is the weakest solid phase increases, the effect of the presence and absence of ITZ was also needed to be evaluated. In Fig. 11, the amount of ITZ elements compared to CP elements in 65 and 281

aggregate porous concretes are presented, where the elements of the selected phase is indicated in red.

It can clearly be seen that the aggregates getting finer drastically increases the portion of ITZ phase in concrete. Therefore, the porous concretes without any ITZ phase should also be analyzed in order to see the individual effect of aggregate size on the material. As it can be seen in Fig.9, when there was no ITZ phase defined, the impact strengths of two porous concretes (with 65 and 281 aggregates) were nearly the same (the peak values were approximately equal).

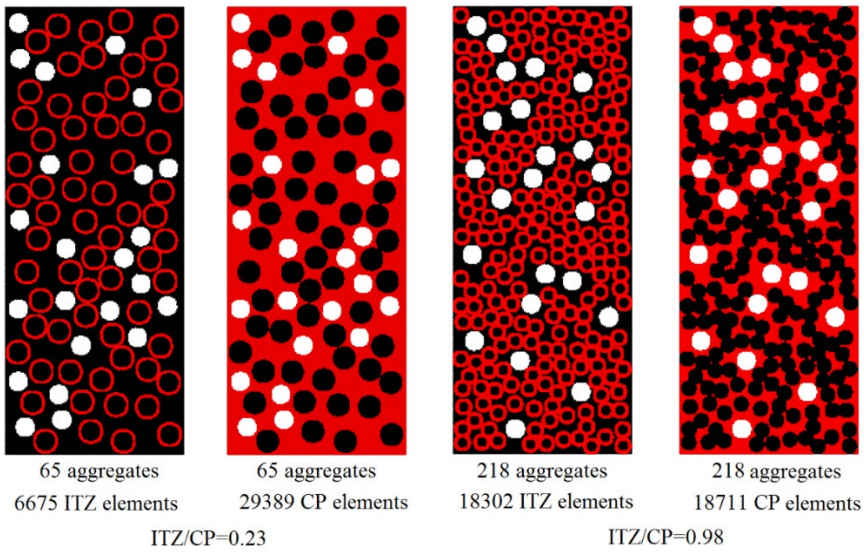

Fig. 11 Distributions of bulk cement paste (CP) and ITZ phases in different mixtures (65AGG23POREITZ (top left), 281AGG23POREITZ (top right), see Table 2) and the corresponding damage contours (bottom)

Therefore, for this set of analyses, it can be said that the effect of aggregate size on the impact strength of porous concretes was negligible unless there is a weak ITZ phase defined around the aggregates which was an important outcome. When this outcome was further checked for the full concretes shown in Fig.7, the same trend was seen. When the aggregate size was decreased while keeping the total amount of aggregates constant, the impact strength stayed the same in case when there was no ITZ phase present (see Fig. 10). In the presence of ITZ however, the impact

strength decreased as the aggregate size was decreased i.e. the number of aggregates were increased from 65 to 218, as can also be seen in Fig. 10.

When the damage contours of porous concretes with 77 pores and 218 or 65 aggregates with ITZ are compared (as seen in Fig. 8), it can be observed that when the aggregate size was decreased, the fragments were generally finer compared to the larger aggregate concrete. However, it can also be observed that in the 281 aggregate porous concrete, in some of the fragments, the aggregates were still bound to each other and stayed intact in groups which increased the fragment sizes at those parts.

For porous concretes, there are several research articles in literature that report their findings on aggregate size having increasing or decreasing effects on the compressive strength of porous concretes [37, 38]. In real porous concretes, the aggregate size and pore size are coupled, i.e. as the aggregates get coarser, the sizes of the pores increase as well. Therefore, the effects of impact strength increasing as the pore size is decreased and decreasing as the aggregate size is decreased (due to the increase in ITZ phase) act simultaneously in real porous concretes. Thus, the information obtained from the analyses conducted on the different sets of model porous concretes, where a single factor is varied while keeping all the other factors constant, in this work cannot be directly verified with experimental data. For real porous concretes, because there are the mentioned factors working simultaneously in opposite directions, each specific mixture should be evaluated separately to see which factors dominate over the others for that individual mixture, which may also explain the controversy in the experimental findings in terms of the effect of aggregate size on strength.

4. Conclusions

The objective of this numerical study was simulating and assessing the dynamic behavior of porous concretes under drop weight impact loading in order to understand the effects of various control parameters individually. The following conclusions can be drawn regarding this work.

- The analyses of the sample with a single pore provided helpful information on the stress and damage distributions at the vicinity of a pore where tensile stress concentrations at the poles and compressive stress concentrations at the sides of the pore were clearly visualized under dynamic compressive loading.

- Model porous concretes with regularly and randomly distributed circular pores were analyzed to better understand the effects of individual parameters associated with pores. From a comparison of the impact responses of model porous concretes with different size pores (constant total porosity), it could clearly be concluded that, with decreasing pore size, the impact strength of the concretes increased. From damage output, it could be concluded that with decreasing pore size (and hence an increase in the number of pores in order to keep the total porosity constant), the sizes of the fragments that are formed drastically decreased. It was also seen in the analyses that increasing the pore size, and consequently increasing the porosity, highly decreased the dynamic strength, as expected.

- In the analyses of porous concretes with randomly distributed circular pores, for each different total number of pores, four random pore distributions were investigated with and without boundary friction between the specimen and the drop weight or the steel plate at the bottom. It could be concluded that when the pore size increased the effect of randomness on the results, i.e. the variance, also increased. Therefore, the results are more reproducible i.e. the production is more easily repeatable, when the pore size is decreased. The analyses with and without end

friction revealed that restrained deformations due to boundary conditions have a major effect on the fragmentation behavior, which was clear from the plots of the damage contour. In case of no friction, no triaxially confined zones were seen while tensile splitting became a more dominant factor.

- Model concretes with randomly distributed aggregates, with/without pores were also analyzed to see the effect of aggregate size on the porous concrete properties with/without the influence of interfacial transition zones. In the analyses, the total amount of aggregates was kept constant while the aggregate size was varied. According to the results, the impact strengths of porous concretes decreased as the aggregate size was decreased when there is also a layer of ITZ defined around the aggregates. However, when there is no ITZ defined, the impact strengths of porous concretes were found to stay approximately the same when the aggregate size is varied. To be able to verify this situation with also full concretes, two different aggregate sizes were also analyzed. It was found that when there is no ITZ, the impact strength stayed the same when the aggregate size was varied. With the presence of ITZ, which is mechanically the weakest phase among the solid phases of concrete, the impact strength decreased as the aggregates got finer, due to the total portion of ITZ increasing with decreasing aggregate size.

- The results obtained from this study show that impact strength increases with decreasing pore size while it decreases with decreasing aggregate size with also the presence of ITZ. In case of real porous concretes, these two factors i.e. pore size and aggregate size, are coupled. During porous concrete production, it was clearly seen that as the aggregate size was increased, the pore size also increased. Because these two coupled factors cause contradicting effects in strength, according to the extent of which factor is more dominant for a specific porous concrete mixture, the effect of that factor may clearly be seen in the strength results for that mixture.

- The numerical model was a versatile tool for the analysis of porous concrete, complementary to experimentation. The analyses provided valuable information which can be used in the design procedure of a porous concrete with predefined requirements.

Acknowledgement

The research presented in this work was conducted at Delft University of Technology and supported by the Netherlands Defense Academy and TNO Defense, Security and Safety.

Compliance with Ethical Standards

Conflict of Interest: The authors declare that they have no conflict of interest.

References

1. Dong H, Gao P, Ye G (2017) Characterization and comparison of capillary pore structures of digital cement pastes. Materials and Structures 50(2),154. https://doi.org/10.1617/s11527-017-1023-9

2. Chen G, Hao Y, Hao H (2015) 3D meso-scale modelling of concrete material in spall tests. Materials and Structures 48:1887–1899. https://doi.org/10.1617/s11527-014-0281-z

3. Agar Ozbek AS, Weerheijm J, Schlangen E, van Breugel K (2013) Dynamic behavior of porous concretes under drop weight impact testing, Cem. and Conc. Comp. 39 1-11. https://doi.org/10.1016/j.cemconcomp.2013.03.012

4. Agar Ozbek AS (2016) Design and Analyses of Porous Concrete for Safety Applications. Dissertation, Delft University of Technology.

5. Chandrappa AK, Biligiri KP (2016) Pervious concrete as a sustainable pavement material-Research findings and future prospects: A state-of-the-art review, Cons. and Build. Mat., 111, 262-274 https://doi.org/10.1016/j.conbuildmat.2016.02.054

6. Lund MSM, Kevern JT, Schaefer VR, Hansen KK (2017) Mix design for improved strength and freeze-thaw durability of pervious concrete fill in Pearl-Chain Bridges. Materials and Structures 50:42. https://doi.org/10.1617/s11527-016-0907-4

7. Sumanasooriya MS, Neithalath N (2011) Pore structure features of pervious concretes proportioned for desired porosities and their performance prediction, Cem. and Conc. Comp. 33 778-787 https://doi.org/10.1016/j.cemconcomp.2011.06.002.

8. Ghafoori N, Dutta S (1995) Building and nonpavement applications of no-fines concrete, J. of Mat. in Civ. Eng, 7(4), 286-9 https://doi.org/10.1061/(ASCE)0899-1561(1995)7:4(286).
9. Timoshenko S, Goodier JN (1987) Theory of Elasticity, McGraw Hill, New York, 1987.
10. Green DJ (1998) An Introduction to the Mechanical Properties of Ceramics, Cambridge University Press., Cambridge.
11. Wong RHC, Lin P, Tang CA (2006) Experimental and numerical study on splitting failure of brittle solids containing single pore under uniaxial compression, Mech. of Mat. 38 (2006) 142-159 https://doi.org/10.1016/j.mechmat.2005.05.017.
12. Wang Y, Wang Z, Liang Y, Du X, Shi Y (2016) Study on the stress and failure strength around the hole in point supported glass panels, Materials and Structures 49:4375–4387 https://doi.org/10.1617/s11527-016-0794-8
13. Sammis CG, Ashby MF (1986) The failure of brittle porous solids under compressive stress states, Acta Metall, 34(3) 511-526 https://doi.org/10.1016/0001-6160(86)90087-8
14. Tang CA, Wong RHC, Chau KT, Lin P (2005) Modeling of compression-induced splitting failure in heterogeneous brittle porous solids, Eng. Frac. Mech. 72 597-615 https://doi.org/10.1016/j.engfracmech.2004.04.008
15. Zhao C, Matsuda H, Morita C, Shen MR (2011) Study on failure characteristic of rock-like materials with an open-Hole under Uniaxial Compression, Strain: An Int. J. for Exp. Mech., 47(5) 405-413 https://doi.org/10.1111/j.1475-1305.2009.00701.x
16. Ashby MF, Sammis CG (1990) The Damage Mechanics of Brittle Solids in Compression, Pure and Appl. Geophy., 133(3) 489-521.
17. Leguillon D, Piat R (2006) Fracture of Porous Materials – Influence of the Pore Size, Eng. Fract. Mech., 75(7) (2006) 1840-1853 https://doi.org/10.1016/j.engfracmech.2006.12.002
18. Susila E, Hryciw RD (2003) Large Displacement FEM Modelling of the Cone Penetration Test (CPT) in Normally Consolidated Sand, Int. J. for Num. and Analytic. Meth. in Geomech., 27(7) 585–602 https://doi.org/10.1002/nag.287
19. Wu SR, Gu L (2012) Introduction to the Explicit Finite Element Method for Nonlinear Transient Dynamics, Wiley, New Jersey.
20. De Borst R, Crisfield MA, Remmers JJC, Verhoosel CV (2012) Non-linear Finite Element Analysis of Solids and Structures, second ed., Wiley, West Sussex.
21. Simulia_1 (2013) ABAQUS Analysis User's Manual 6.13.

22. Lubliner J, Oliver J, Oller S, Oñate E (1989) A Plastic-Damage Model for Concrete, Int. J. of Sol. and Struct, 25(3) 229-326 https://doi.org/10.1016/0020-7683(89)90050-4

23. Lee J, Fenves GL, A Plastic Damage Model for Cyclic Loading of Concrete Structures, ASCE J. of Eng. Mech., 124 (1998) 892–900 https://doi.org/10.1061/(ASCE)0733-9399(1998)124:8(892)

24. Hillerborg A, Modeer M, Petersson PE (1976) Analysis of crack formation and crack growth in concrete by means of fracture mechanics and finite elements, Cem. and Conc. Res. 6 (1976) 773–782 https://doi.org/10.1016/0008-8846(76)90007-7

25. Chaudhari SV, Chakrabarti MA (2012) Modeling of Concrete for Nonlinear Analysis Using Finite Element Code ABAQUS, Int. J. of Comp. Appl. 44(7) (2012) 14-18. https://doi.org/10.5120/6274-8437

26. Jankowiak T, Lodygowski T (2005) Identification of Parameters of Concrete Damage Plasticity Constitutive Model, Found. of Civ. and Env. Eng. 6 53-69.

27. Kmiecik P, Kaminski M (2011) Modelling of Reinforced Concrete Structures and Composite Structures with Concrete Strength Degradation Taken into Consideration, Arch. of Civ. & Mech. Eng., 11(3) 623-636 https://doi.org/10.1016/S1644-9665(12)60105-8

28. Sun JS, Lee KH, Lee PH (2000) Comparison of Implicit and Explicit Finite Element Methods for Dynamic Problems, J. of Mat. Process. Tech. 105(1-2) 110-118 https://doi.org/10.1016/S0924-0136(00)00580-X

29. Martin O (2010) Comparison of different constitutive models for concrete in ABAQUS/Explicit for missile impact analyses, JRC European Commission.

30. Rousakis TC, Karabinis AI, Kiousis PD. (2007) FRP-confined concrete members: Axial compression experiments and plasticity modeling. Eng Struct 29

31. Chen, W. F., & Han, D. J. (1988) Plasticity for Structural Engineers Springer-Verlag New York.

32. Gorst NJS, Williamson SJ, Pallett PF, Clark LA (2003) Friction in temporary works, Research Report, University of Birmingham, U.K.

33. Deutsches Institut für Normung (1982) Falsework calculation, design and construction DIN 4421:1982, Beuth Veriag GmbH, Berlin.

34. British Standards Institution (1997) Falsework performance requirements and general design, Draft prEN 12812, London, U.K.

35. J.G.M. van Mier (2013) Concrete Fracture: A Multiscale Approach, CRC Press, USA.
36. Schulson M, Iliescu D, Renshaw CE (1999) On the initiation of shear faults during brittle compressive failure: A new mechanism, J. of Geophy. Res. 104 695-705 https://doi.org/10.1029/1998JB900017
37. Chindaprasirt P, Hatanaka S, Mishima N, Yuasa Y, Chareerat T (2009) Effects of binder strength and aggregate size on the compressive strength and void ratio of porous concrete, Int. J. of Min., Metal. and Mat., 16(6) 714-719 https://doi.org/10.1016/S1674-4799(10)60018-0
38. Deo O, Neithalath N (2010) Compressive behavior of pervious concretes and a quantification of the influence of random pore structure features, Mat. Sci. and Eng.: A 528(1) 402-412 https://doi.org/10.1016/j.msea.2010.09.024